Supplementary Materials

The supplement contains 3 tables (Tables S1-S3) and 5 figures (Figures S1-S5). Table S1 summarizes the ratio of the afterslip and coseismic moment release and the position of afterslip relative to the coseismic slip from previous studies. Table S2 summarizes the rheologic structures inferred in previous studies. Table S3 shows the range, optimal and uncertainties of InSAR-inversion fault slip parameters for the afterslip for time period 2.

Figure S1 shows the coseismic displacement field for the aftershock of 25 August 2018. Figure S2 shows the uniform slip inversion result for the afterslip model for time period 2. Figure S3 shows a conceptual model of the fault spatial relationships. Figures S4 and S5 show the sampled data used for modelling of the aftershocks, and for the afterslip and viscoelastic relaxation processes.

Table S1. Reported ratio of afterslip moment release relative to the coseismic moment release and the position of afterslip relative to the coseismic slip.

Earthquake	Coseismic Magnitude	Studied post-seismic time period	Position of afterslip	Ratio of afterslip to Coseismic moment Magnitude released	Reference
Continental earthquakes					
1989 Loma Prieta	Mw 7.1	8 years	Up-dip	7%	Segall et al., 2000
1992 Landers	Mw 7.3	6 months	Down-dip	15%	Shen et al., 1994
1994 Northridge	Mw 6.7	1.5 years	Up-dip	22%	Donnella et al., 1998
1994 Sefidabeh	Mw 6.5	8 years	Up-dip and overlap with coseismic slip	9%	Copley et al., 2014
1997 Manyi	Mw 7.5	3 years	Down-dip	20%	Ryder et al., 2007
1999 Izmit	Mw 7.5	87 days	Down-dip and overlap with coseismic slip	22%	Burgmann et al., 2002;
1999 Hector Mine	Mw 7.1	1 year	Up-dip	5%	Jacobs et al., 2002a
1999 Chi-Chi	Mw 7.6	3 months	South and down-dip of the largest coseismic slip	7%	Hsu et al., 2002
2000 Iceland earthquakes	2*Mw 6.5	4 years	Down-dip	30%	A´ rnado´ttir et al., 2005.
2002 Denali	Mw 7.9	4 year	Down-dip	0.8%	Gomberg et al., 2012
2003 Bam	Mw 6.6	3.5 years	Up-dip and to the south of the largest coseismic slip	3%	Fileding et al., 2009
2003 Boumerdes	Mw 6.9	2.5 years	Up-dip	31%	Mahsas et al., 2008
2003 San Simeon	Mw 6.5	10 months	Up-dip	14%	Johanson et al., 2010

2003 Zemmouri	Mw 6.8	7 years	Up-dip and overlap with coseismic slip	17.8%	Cetin et al., 2012
2003 Chengkung	Mw 6.8	157 days	Up-dip	13%	Hsu et al., 2009
2004 Parkfield	Mw 6.0	2 years	Up-dip and overlap with coseismic patch	280%	Freed et al., 2007.
2005 Chaman	Mw 5.0	543 days	Down-dip	560%	Furuya et al., 2008
2005 Pakistan	Mw 7.6	1500 days	Down-dip	56%	Jouanne et al., 2011
2007 Ghazaband	M 5.5	1 year	Up-dip	70%	Fattahi et al., 2015
2008 Wenchuan	Mw 7.9	7 years	Down-dip	25%	Diao et al., 2018
2008 Damxung Tibet	Mw 6.3	1.6 years	Down-dip and overlap with coseismic patch	11%	Bie et al., 2014
2008 Nima-Gaize	Mw 6.4	9 months	Overlap with coseismic patch	10%	Ryder et al., 2010
2009 L'Aquila	Mw 6.3	180 days	Overlap with coseismic patch	18%	D' Agostino et al., 2012
2010 El Mayor Cucapah	Mw 7.2	5months	periphery of the main coseismic slip patches	11.5%	Alejandro et al., 2013
2014 Napa	M 6.0	I year	along the southern part of the rupture at depths<=5km	32.5%	Pollitz et al., 2019
2015 Gorkha	Mw 7.9	2 years	Down-dip	10%	Wang et al., 2018
2016 Kaikoura	Mw 7.8	6 months	Up-dip and Down-dip	14%	Jiang et al., 2018
Subduction earthquakes					
1995 Antofagasta	Mw 8.0	5 years	Down-dip and some overlap with coseismic slip	<20%	Pritchard et al., 2006
1995 Jalisco	Mw 8.0	4 years	Down-dip	70%	Hutton et al., 2001
2001 Peru	Mw 8.4	1 year	Down-dip	25%	Ruegg et al., 2002.
2003 Tokachi-oki	Mw 8.1	1 year	U-shape and circleing the coseismic patches	61%	Baba et al., 2006
2004 Sumatra–Andaman	Mw 9.15	40 days	Down-dip	30%	Chlieh et al., 2007
2005 Nias-Simeulue	Mw 8.7	11 months	Up-dip	18%	Hsu et al., 2006
2007 Pisco, Peru	Mw 8.0	408 days	Nearby coseismic patches	28%	Perfettini et al., 2010

2010 Maule	Mw 8.8	1.3 years	Down-dip	20-30%	Lin et al., 2010
2011 Tohoku-oki	Mw 9.0	2.5 years	Down-dip	28%	Yamagiwa et al., 2014

Table S2. Rheologic structures in previous studies.

Earthquakes	Coseismic magnitude	Studied post-seismic time period	Layers model	Rheology	Viscosity (Pas)	Reference
Viscoelastic relaxation occurred on upper mantle						
1915-1954 Central Nevada Seismic Belt (CNSB)	sequences	8 years	Upper crust	Elastic		Gourmelen et al., 2005
			Lower crust	Maxwell	$>10^{20}$	
			Upper mantle	Maxwell	$1-7\times10^{18}$	
1959 Hebgan Lake	Mw 7.3	27 years	Crust	Elastic		Nishimura et al., 2003
			Viscosity half space	Maxwell	$4\times10^{18\pm0.5}$	
1992 Landers	Mw 7.3	0.25-3years	Upper crust	Elastic		Pollitz et al., 2000
			Lower crust	SLS	1.6×10^{19}	
			Upper mantle	Maxwell	8×10^{18}	
1999 Hector Mine	Mw 7.1	9 months	Upper crust	Elastic		
			Lower crust	Maxwell	10^{19} & $\eta_{lc}\geq\eta_{um}$	Pollitz et al., 2001 Science
			Upper mantle	Maxwell	10^{17}	
2000 Iceland earthquakes	2*Mw 6.5	5 years	Upper crust	Elastic		Jonsson et al., 2008
			Lower crust	Maxwell	$3-4\times10^{19}$	
			Upper mantle	Maxwell	10^{18}	
2002 Denali	Mw 7.9	2.5 years	Crust	Elastic		Biggs et al., 2009
			Upper mantle	Maxwell	10^{18}	
2010 El Mayor Cucapah	Mw 7.2	1.5 years	Upper crust	Elastic		Pollitz et al., 2012
			Lower crust	Maxwell	10^{19}	
			Upper mantle	Burgers	Steady: 10^{18} Transient: 10^{17}	
Viscoelastic relaxation occurred on lower crust and upper mantle						

1999 Izimit Turkey	Mw 7.5	6 years	Upper crust	Elastic		Wang et al., 2009b
			Lower crust	SLS	2×10^{18}	
			Upper mantle	Maxwell	7×10^{19}	
Viscoelastic relaxation occurred on lower crust						
1980 Italy Irpinia	Mw 6.9	2-5 years	Upper crust	Elastic		Dallavia et al., 2005
			Lower crust	Maxwell	10^{19}	
			Upper mantle	Maxwell	Cannot constrain	
1989 Loma Prieta	Mw 7.1	5 years	Upper crust	Elastic		Pollitz et al., 1998
			Lower crust	Maxwell	10^{19}	
			Upper mantle	Maxwell	Strong mantle	
1990 Gonghe	Mw 6.4		Upper crust	Elastic		Hao et al., 2012
			Lower crust	Maxwell	9×10^{19}	
			Upper mantle	Maxwell	9×10^{19}	
1994 Northridge	Mw 6.7	2.9 years	Upper crust	Elastic		Deng et al., 1999
			Lower crust	Maxwell	10^{18}	
			Upper mantle	Maxwell	10^{20}	
1997 Italy Umbria Marchf sequence	Mw 5.6 - 6	2-6 years	Upper crust	Elastic		Riva et al., 2007
			crustal transition zone	Maxwell	10^{18}	
			Lower crust	Maxwell	Strong mantle	
1997 Manyi	Mw 7.5	4 years	Upper crust	Elastic		Ryder et al., 2007
			Lower crust	SLS	4×10^{18}	
			Upper mantle	elastic		
1999 Chi-Chi	Mw 7.6	3 months	Upper crust	Elastic		Sheu et al., 2004
			Lower crust	Maxwell	10^{17}	
			Upper mantle	Maxwell	Strong mantle	
2001 Kokoxili	Mw 7.9	5 years	Upper crust	Elastic		Ryder et al., 2011
			Lower crust	Burgers	Steady: 10^{19} Transient: 10^{17}	
			Upper mantle	elastic		

2001 Bhuj	Mw 7.6	6 years	Crust	Elastic		Reddy et al., 2013
			Viscosity half space	Maxwell	$1-2\times10^{19}$	
2003 Bam	Mw 6.6	5 years	Elastic layer			Wimpenny et al., 2017
			Viscosity half space	Maxwell	$\geq 10^{19}$	
2004 Parkfield	Mw 6.0	6 years	Upper crust			Bruhat et al., 2011
			Viscosity half space	Maxwell	10^{18}	
2008 Wenchuan	Mw 7.9	7 years	UC: Tibet/Sichuan	Elastic		Diao et al., 2018
			LC: Tibet/Sichuan	Maxwell	$10^{18}/\geq 10^{20}$	
			UM: Tibet/Sichuan	Maxwell	$10^{19}/10^{20}$	
2008 Damxung Tibet	Mw 6.3	615 days	Elastic layer	Elastic		Bie et al., 2014
			Viscosity half space	Maxwell	10^{18}	
Mongolia 20th earthquakes		1994-2002	Upper crust	Elastic		Vergnolle et al., 2003
			Lower crust	Maxwell	Less well constrained: $3\times10^{16}-2\times10^{17}$	
			Upper mantle	Maxwell	$1-4\times10^{18}$	

Table S3. Range, optimal and uncertainties of InSAR-inversion fault slip parameters for the afterslip for time period 2.

	Length (km)	Width (km)	Depth (km)	Dip (°)	Strike (°)	Dip slip[b] (m)	Strike slip[c] (m)	Lat[d,e]	Lon[d,e]	Mw[e]	rms(m)
Lower	5	0	0.5	-40	330	0	-3	—	—	—	
Upper	100	50	45	40	360	5	3	—	—	—	
Optimal	**57.0**	**0.4**	**8.9**	**-33**	**346**	**2.5**	**-1.7**	**34.50**	**45.69**	**6.22**	**0.025**
2.5%	46.8	0.2	7.3	-38	343	0.4	-2.7	—	—	—	
97.5%	74.1	1.3	11.3	-19	348	4.7	1.2	—	—	—	

[a] maximum posteriori probability solutions of 2.5% and 97.5% from the posterior probability density function of fault parameters. [b] the positive value means the hanging wall showed relative uplift; [c] the negative value means that the hanging wall direction of the motion was opposite to the strike; [d] longitude and latitude of the corner of upper edge; [e] calculated based on the optimal inversion parameters.

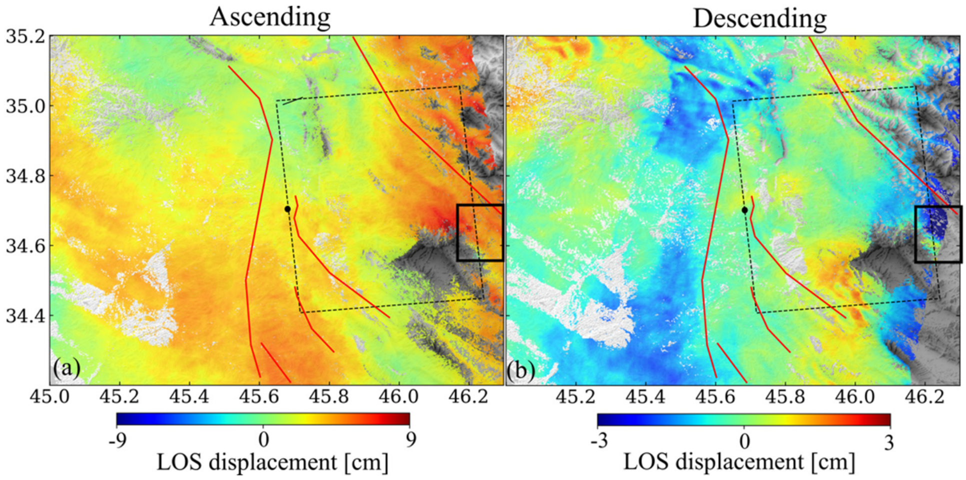

Figure S1. Coseismic displacement field caused by the aftershock of 25 August 2018. (a) Ascending data from 20 August 2018 to 26 August 2018. (b) Descending data from 21 August 2018 to 2 September 2018. Black dashed rectangle: coseismic fault; black dot: upper edge of fault; black solid rectangle: coseismic deformation region caused by 25 August 2018 aftershock.

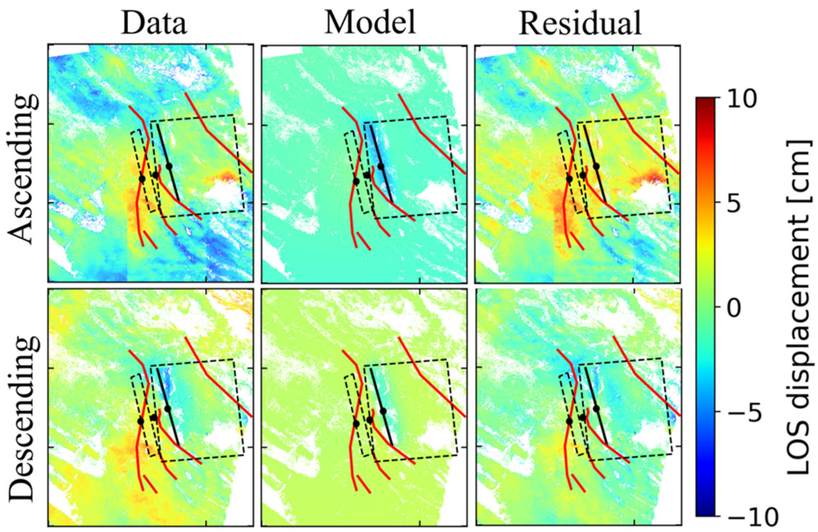

Figure S2. Uniform slip inversion result for afterslip for time period 2. Black dash rectangles: afterslip fault for time period 1 and coseismic fault, respectively; black dot: upper edge of fault; black solid rectangle: best-fitting afterslip fault for time period 2. The solid rectangle closes to a solid line due to the small width of the fault.

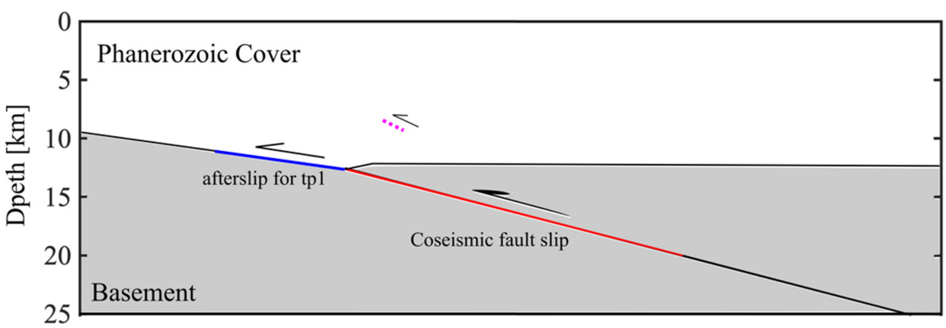

Figure S3. Conceptual model of the spatial relationship between coseismic fault slip (red line) and afterslip for time period 1 (blue line). The best-fitting afterslip model for time period 2 is also shown (dashed magenta line). That it is located within the phanerozoic cover is another reason that we discard this model.

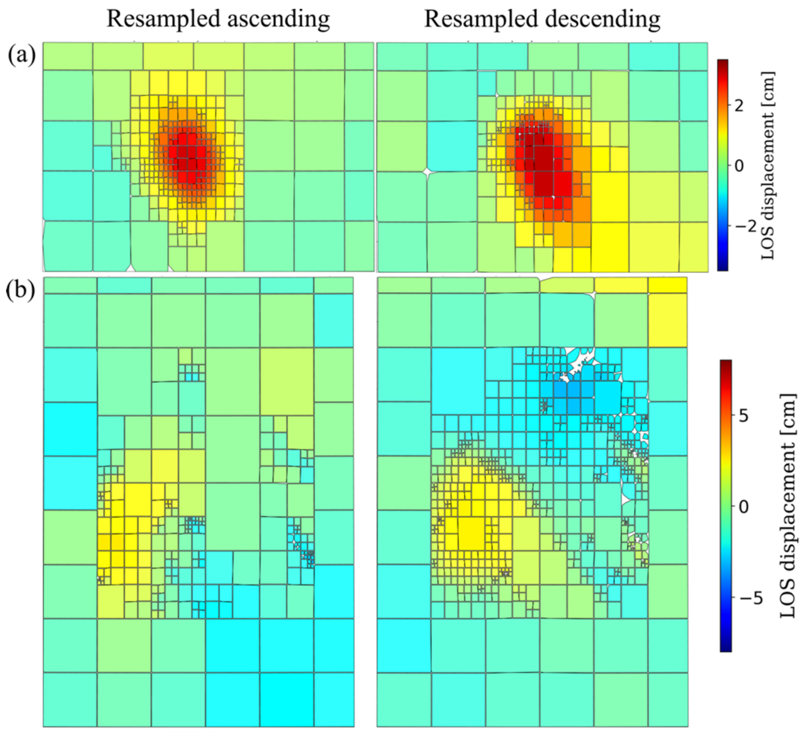

Figure S4. Sampled data used for modelling (left: ascending data, right: descending data). a):aftershock sequence 1; b) aftershock sequence 2.

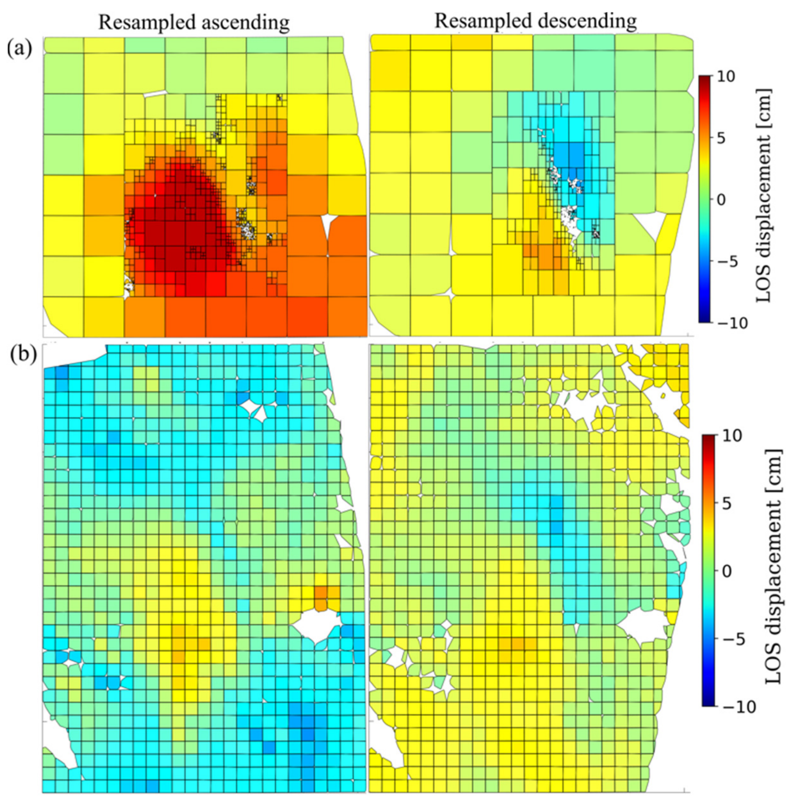

Figure S5. Same as Fig. S4 but for a) time period 1 and b) time period 2 (we obtained the same results using combined downsampling).